

Article

Structural and Photoprotective Characteristics of Zn-Ti, Zn-Al, and Mg-Al Layered Double Hydroxides—A Comparative Study

Orielia Pria Egambaram ^{1,2,3} , Sreejarani Kesavan Pillai ^{1,*} , Suprakas Sinha Ray ^{1,2}  and Marelize Goosen ⁴

¹ DST/CSIR Centre for Nanostructures and Advanced Materials, Council for Scientific and Industrial Research, Pretoria 0001, South Africa; o.egambaram@kent.ac.uk (O.P.E.); rsuprakas@csir.co.za (S.S.R.)

² Department of Chemical Sciences, University of Johannesburg, Johannesburg 2028, South Africa

³ Division of Natural Sciences, University of Kent, Canterbury CT2 7NH, UK

⁴ Photobiology Laboratory, Sefako Makgatho University, Pretoria 0204, South Africa; marelize.lategan@smu.ac.za

* Correspondence: skpillai@csir.co.za; Tel.: +27-12-8413759

Abstract: Organic UV filters have been known to generate harmful by-products and undergo photoreactive degradation, which ultimately poses a great threat to consumers using sunscreen products. Inorganic UV filters such as TiO₂ and ZnO, although considered safer options, are not without threat considering their photocatalytic nature and ability to generate reactive oxygen species. A study was conducted to identify the influence of different metal ions on the photochemical properties of layered double hydroxides (LDH), Zinc-Titanium LDH (Zn-Ti LDH), Zinc-Aluminium LDH (Zn-Al LDH), and Magnesium-Aluminium LDH (Mg-Al LDH) and their prospects in photoprotection. The photocatalytic properties of the LDH were analyzed and compared to TiO₂ and ZnO. The intermediate band gaps of Zn-Ti (3.72 eV) and Zn-Al LDH (3.3 eV) proved favorable and safer for the use of these LDH in cosmetic formulations as they offer lower photo-reactivity when compared to cosmetic grade ZnO and TiO₂. The *in vitro* SPF values obtained for formulations containing 2 wt% Zn-Ti and 2 wt% Zn-Al LDH showed promise, with both samples claiming “broad spectrum” protection and valid claims of UVA protection.

Keywords: layered double hydroxides; bandgap; diffuse reflectance; methylene blue degradation; photo-reactivity



Citation: Egambaram, O.P.; Kesavan Pillai, S.; Ray, S.S.; Goosen, M. Structural and Photoprotective Characteristics of Zn-Ti, Zn-Al, and Mg-Al Layered Double Hydroxides—A Comparative Study. *Cosmetics* **2023**, *10*, 100. <https://doi.org/10.3390/cosmetics10040100>

Academic Editor: Antonio Vassallo

Received: 8 June 2023

Revised: 3 July 2023

Accepted: 4 July 2023

Published: 7 July 2023



Copyright: © 2023 by the authors. Licensee MDPI, Basel, Switzerland. This article is an open access article distributed under the terms and conditions of the Creative Commons Attribution (CC BY) license (<https://creativecommons.org/licenses/by/4.0/>).

1. Introduction

There are ongoing discussions worldwide on the adverse side effects of current sunscreen ingredients (both organic and inorganic), and the sun protection product market is showing a paradigm shift towards more environmentally/skin-friendly and sustainable ingredients as a possible replacement. Commercial sunscreen products widely use inorganic sunscreen ingredients with relatively more structural stability, namely micro and nanoparticles of TiO₂ and ZnO. However, these are known photocatalysts and their photocatalytic activity under sunlight could present serious human and environmental toxicity. Hence, it is essential to develop efficient inorganic nanostructures as UV-protective materials with lower photoreactivity, good physical stability, and superior UV reflection/scattering characteristics. Nanostructured clay minerals represent emerging inorganic nanoparticles with photoprotection capacity, which was explored in different applications, such as in cosmetic formulations [1,2].

Layered double hydroxides (LDH) are two-dimensional clay minerals that are either naturally occurring or synthetically produced and are comprised of inorganic elements. LDHs are materials which have the basic structure based on brucite-like layers with the formula (M^{II}(OH)₂). The general formula for LDH is [M^{II}_{1-x}M^{III}_x(OH)₂]^{x+} · [(Aⁿ⁻_{x/n}) · mH₂O]^{x-}, where M^{II} and M^{III} represent the divalent and trivalent cations and Aⁿ⁻ represents the

interlayer anion. The coefficient x is the molar fraction, $[M^{III}/(M^{II} + M^{III})]$ [3]. The stoichiometric ratio of $0.20 < x < 0.33$ was perceived as ideal for LDH formation; however, it has been found that LDH can be formed outside this range, and these have multiple crystalline phases [4]. LDH surface is positively charged owing to the presence of different metal cations, and the overall electroneutrality of the LDH is due to anions present in the interlayer that counterbalance the positive charge of the structure [5].

Given that the structure of LDH is closely related to that of $Mg(OH)_2$, the replacement of Mg^{2+} requires a cation with an ionic radius close to that of Mg^{2+} . However, several pieces of the literature prove this to be contrary; most importantly, these include the incorporation of Cu^{2+} , which was thought to have undergone Jahn–Teller distortions when incorporated in the LDH structure [6]. LDH can be synthesized using Mg^{2+} , Zn^{2+} , Ni^{2+} , Cu^{2+} , Al^{3+} , Fe^{3+} , Ti^{4+} , and Sn^{4+} . Ternary or quaternary LDH may be formed with different cations, and these LDH have varying stability due to the cations present where the most stable divalent cation is Zn^{2+} [4]. The incorporation of different cations also influences the electrostatic forces within the LDH, which may have further effects on its crystallinity and anion exchange capacity. Increasing the number of cations creates stronger electrostatic interactions between cations and the coordinated OH^- anions [4].

LDH have a hexagonal close-packed structure. Metal cations are found in octahedral holes between alternating OH planes. The local geometry of the metal cation is D_{3d} . The literature states that in pure LDH, the unit cell parameter a might be an indication of non-stoichiometry. In an ideal octahedron, $a = 2^{1/2} \times r(M-O)$. A constant distortion exists for the unit cell parameters and the M-O distances [6]. Furthermore, as the metal ionic radius increases, the thickness of the interlayer space h decreases, which also decreases the parameter a [7]. For LDH that contains Mg and Al, it has been reported that the unit cell parameter a decreases as the value of x increases due to the smaller size of Al^{3+} , in comparison to Mg^{2+} . This is in correlation with Vegard's Law [3].

LDH can be prepared using various methods; co-precipitation at constant pH, urea hydrolysis, sol-gel method, hydrothermal synthesis, ion exchange, reconstruction, or mechanical milling [4,8]. All preparation methods are essentially based on using a base to displace the anions from a precursor, leading to the incorporation of these anions within the LDH structure [4,9]. Synthetic methods influence the particle size and crystallinity, and hence, the properties of LDH [5,10]. The formation of LDH, in turn, is influenced by pH, concentration, nature of the base, ageing time, temperature, total cation concentration, and the ratio between M^{II} and M^{III} ions [10].

LDH have a wide array of uses across several fields that include use as catalysts, ion exchangers, or absorbents. The diversity of their usage is based on unique properties of LDH such as memory effect, anionic exchange, tuneable porosity, easily manipulated structure, basic character due to the hydroxylated surfaces, and cations dispersed within the layered sheets [4,10]. LDHs have often been used as photocatalysts due to their high anion retention capacity, making them efficient for the removal of organic matter from wastewater [10,11]. The octahedral organization of the MO_6 groups in the layer allows LDH to act like doped semiconductors [12]. At the same time, the tuneable chemical composition presents the opportunity to manipulate the bandgap of these materials and hence the light absorption properties. The photocatalytic properties of the Zn-Al LDH are described to be directly proportional to the amount of Zn present within the LDH, which may be varied by changing the Zn/Al ratio or the reaction temperature [10,11,13,14].

Due to the negative side effects of the current sunscreen ingredients (carcinogenicity, endocrine disrupting nature, bioaccumulation, marine and coral reef pollution and damage, photoreactivity, and toxicity), the sun protection product market is showing a paradigm shift towards more environmentally friendly and sustainable ingredients as a solution, with an interest to attract emerging consumer markets that prefer natural products [15]. Primary prevention is considered the most cost-effective route to minimize the skin cancer burden in countries that experience extreme levels of UV radiation, such as South Africa, Australia, New Zealand, etc. [16]. Sunscreens are an effective primary prevention measure; however,

there is a huge demand for new environmentally and skin-friendly, non-photocatalytic UV filters that can offer effective sun protection. Reports have highlighted the use of LDH in photoprotection as a matrix to intercalate organic UV filter ingredients to improve photostability and slow-release properties [17–19]. The biocompatibility of LDH is well documented [20–22], and Mitter et al. [23] concluded that LDH degradation occurs gradually under atmospheric CO₂ and moisture, which makes them environmentally friendly materials. The applicability of LDH as UV-blocking materials in various polymer matrices also has been investigated [24–26], where incorporation of various cations showed changes in the UV filtering characteristics of the composite structures. However, studies on the applicability of pristine LDH in photoprotective topical formulations are scarce. Our group recently reported the prospects of Zn-Ti LDH in o/w sunscreen formulations [9].

This article seeks to characterize the UV protective properties of a number of layered double hydroxides (LDH). In this study, we investigated the effect of incorporating different cations on their physical, optical, and photochemical properties of LDH and sun protection characteristics of formulations prepared using these materials. The optical and photochemical properties of LDH prepared were compared to that of cosmetic grade TiO₂ and ZnO, which are inorganic UV filters widely used in sun protective formulations currently. The observations from the study are envisaged to add value to the development of new-generation UV-shielding materials with lower environmental impact while ensuring consumer skin health and safety.

2. Experimental Section

2.1. Materials

Unless otherwise stated, all chemicals and reagents were used as received. Zinc Nitrate Hexahydrate (98%), Titanium Isopropoxide (99.9%), Urea (99.8%), Aluminium Nitrate Nonahydrate (98%) were obtained from Sigma Aldrich, South Africa. Sodium Hydroxide (98%) was purchased from Merck, Johannesburg, South Africa. Cosmetic grade nano-ZnO and nano-TiO₂ were kindly provided by AMKA Pty Ltd., Pretoria, South Africa. Commercial Mg-Al LDH was obtained from Sasol, Sasolburg, South Africa.

2.2. Methods

2.2.1. Synthesis of LDH

For preparing Zn-Al LDH, Zinc Nitrate Hexahydrate (0.2 mol) and Aluminum nitrate nonahydrate (0.1 mol) were dissolved in 200 mL of deionized water. Once completely dissolved, sodium hydroxide (2M) was added dropwise to keep the pH at 10 under stirring at room temperature (25 °C) for 24 h. Thereafter, the mixture was aged for 24 h and then centrifuged. The precipitate obtained was washed and dried at 60 °C for 24 h in the air oven. The synthesis method of Zn-Ti LDH is as per the method described in our previous work [9]. In a typical experiment, the metal salt precursors—zinc nitrate hexahydrate (0.004 mol), titanium isopropoxide (0.001 mol), and urea (0.05 mol)—were dissolved in 100 mL deionized water and stirred vigorously at 120 °C for 24 h. The solution thereafter was aged at room temperature (25 °C) for 24 h. The mixture was centrifuged at 4000 rpm for 6 min and washed with distilled water many times. The solid residue was at last rinsed with acetone and dried in a vacuum oven at 120 °C. The LDH precipitate was then ground, sieved to 75 μm, and kept in an airtight container for further analyses and experiments. Commercial grade Mg-Al LDH used in this study was synthesized by hydrolysis of heterometallic alcoholates with a Mg:Al ratio of 3:1 as per the specification sheet.

2.2.2. Characterisation

Powder XRD was carried out on a PANalytical X'Pert PRO instrument, using a Cu K α (1.5406 Å) radiation at 45 kV and 40 mA to obtain crystallographic information. The scan range was between a two-theta of 0° and 75°, with a step size of either 0.02° or 0.01°. The morphology of the LDH materials was studied using SEM on a JEOL-JSM 7500F (Jeol,

Tokyo, Japan) with an accelerating voltage of 3.0 kV and an emission current of 10 μA . FTIR spectra were acquired using a Perkin Elmer Spectrum 100 FTIR spectrometer (Perkin Elmer, Waltham, MA, USA) with the MIRacle ATR attachment and a Zn/Se crystal at a spectral resolution of 4 cm^{-1} . The FTIR measurements were performed with a scan range of 4000–600 cm^{-1} . TGA (TGA Q500 (TA instruments, New Castle, DE, USA) was used to determine the thermal stability of the various LDH with a temperature ramp from room temperature to 900 $^{\circ}\text{C}$ with a ramp of 10 $^{\circ}\text{C}/\text{min}$ in an air atmosphere with a flow rate of 60 mL/min. BET surface analysis was conducted using a TRISTAR 3000 (Micrometrics, Norcross, GA, USA) surface area analyzer. The samples were degassed for 2 h prior to the analysis. XPS Analysis was conducted to determine the oxidation state of the metals present on the surface. Analysis was conducted at the National Metrology Institute of South Africa (NMISA) on a Thermo ESCALab 250Xi instrument (Thermo Fisher Scientific Corporation, Waltham, MA, USA) using 300 W monochromatic Al $K\alpha$ (1486.7 eV) X-rays. The X-ray spot size was 900 μm .

2.2.3. Optical Properties

The optical properties of the synthesized materials were analyzed using DRUV-Vis Spectroscopy. This was conducted using a Perkin Elmer Lambda 950 UV-Vis spectrometer (Perkin Elmer, Waltham, MA, USA) with a 150 mm integration sphere, between 200 and 1000 nm wavelength range with a resolution of 1 nm. Cosmetic-grade nano-TiO₂ and nano-ZnO were used as reference samples. The data collected from the DR UV-Vis spectra were used to obtain Kubelka–Munk (K–M) plots which provided information about the material's absorbance in the UV region. This was performed using the equation given below, where R is the value of the absolute reflectance of the samples.

$$F(R) = \left(\frac{(1 - R)^2}{2R} \right) \quad (1)$$

Tauc plots were obtained from K–M plots to determine the band gap of different LDH prepared.

2.2.4. Measurement of Photochemical Activity

The photocatalytic activity of the synthesized materials was analyzed by employing Methylene Blue (MB) photodegradation under ultraviolet light ($\lambda = 254 \text{ nm}$ and 365 nm) irradiation. Cosmetic grade ZnO and TiO₂ were used as reference samples. The UV light source was a 6 W UV GL-58 handheld UV lamp with a 254 or 365 nm wavelength pass filter. The extent of degradation of MB at 365 nm and 254 nm was used to gauge the photoreactivity of LDH adequately.

In a typical experiment, 6 mg of LDH sample was dispersed in 75 mL of 5 ppm MB solution (0.08 mg/mL). The adsorption/desorption equilibrium was allowed to reach by stirring the mixture in the dark for 30 min. UV-Vis analysis prior to UVR exposure was conducted on each sample to determine the initial concentration (C_0). The solutions were then stirred vigorously under UVR (either 365 nm or 254 nm). At definite time intervals, a 3 mL aliquot of mixture was taken from each beaker while replacing it with 3 mL distilled water. The filtrate was analyzed using UV-Vis spectrometry at 25 $^{\circ}\text{C}$ using a Perkin-Elmer 750 s UV-Vis spectrometer (Perkin Elmer, Waltham, MA, USA) with a wavelength scan ranging from 700 to 200 nm. The maximum absorption band for MB was measured at 664 nm.

2.2.5. *In-Vitro* SPF Measurement

Zn-Al and Zn-Ti LDH were incorporated into o/w sunscreen emulsion with 2 wt% loading and the samples were stored in the dark after preparation (Table S1 in the Supplementary Materials). A specified amount of sample is spread onto a polymethylmethacrylate (PMMA) plate, and an *in vitro* transmission measurement was taken in replicates before

irradiation. The PMMA plates were then irradiated using a Labsphere UV Transmittance Analyser 2000S (Labsphere, North Sutton, NH, USA), and SPF characteristics were measured as per the testing procedure outlined by ISO 24443.

3. Results and Discussion

3.1. Characterization of LDH

The XRD patterns for the different LDHs (Figure 1) indicate that all three LDHs are crystalline materials and exhibit the characteristic reflections of LDH with planes (003), (006), and (009) [4,27]. As seen in Figure 1, the (003) basal reflection, the most intense reflection, is indicative of the LDH structure. This reflection typically occurs at approximately $2\theta = 11.7^\circ$ corresponding to a d-spacing of 7.6 Å for natural and synthetic LDH with carbonate anion in the interlayer space, and this was consistent with findings for Zn-Al and Mg-Al LDH (Figure 1) [5,14,28]. However, the (003) basal reflection was moved to $2\theta = 12.88^\circ$ ($d_{003} = 6.85$ Å) for Zn-Ti LDH. As explained in our previous work [9], this shift was due to the incorporation of Ti^{4+} into the LDH structure. The shift in 2θ angle was complemented by an overall decrease in the basal spacing, which may be associated with the strong electrostatic interactions existing between the carbonate interlayer anion and the host layer [5]. The presence of Ti^{4+} in Zn-Ti LDH results in less repulsion between the layers in comparison to the LDH containing Al^{3+} , allowing stronger electrostatic attraction between the anion and cation which draws the layers closer [14]. Peaks observed at $2\theta \approx 32^\circ$ and 35.7° (peaks marked with “+” sign) correlate to $Zn(OH)_2$ as substantiated by PDF card 00-020-1437 [5].

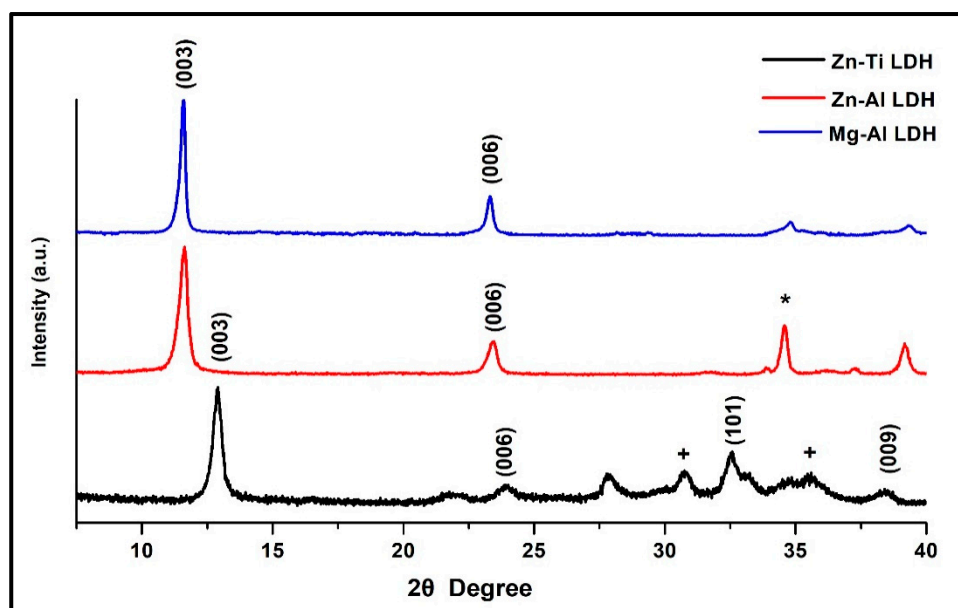


Figure 1. Powder XRD patterns of LDH with different cations. +: corresponds to $Zn(OH)_2$ peaks confirmed by PDF card 00-020-1437. *: Corresponds to (009) basal reflection of Zn-Al LDH.

The structures of Zn-Al and Mg-Al were expected to have a high degree of similarity due to their similar cationic radii and the electrostatic repulsion exhibited by these cations. Zn^{2+} has an ionic radius of 0.074 nm, compared to 0.065 nm of the ionic radius of Mg^{2+} [6]. A slight shift in (003) reflection to the right observed for Zn-Ti LDH herein is reportedly due to the isomorphic substitution of Zn^{2+} ions by tetravalent Ti^{4+} ions. The ionic radius of Al^{3+} is smaller than that of Ti^{4+} (0.064 nm), which could not explain the shift of (003) reflection to a higher 2θ angle [5,14,29]. A less intense (006) reflection is observed for Zn-Ti LDH in comparison to Zn-Al and Mg-Al LDH, and similar observations were reported by Seftel et al. [30]. Despite the shift in the (003) reflection for Zn-Ti LDH, (006) reflections which were observed at $2\theta = 23^\circ$ did not experience any shifts [5]. Zn-Al LDH showed a

minor trace of the ZnO phase at $2\theta = 34.7^\circ$ [30]. The experimental XRD pattern of reference TiO_2 agrees well with the JCPDS card no. 21-1272 of the anatase phase of TiO_2 (Figure S1 in Supplementary Materials). The spectrum with peaks at $2\theta = 25.4^\circ, 38.1^\circ, 48.1^\circ, 54.3^\circ, 55.4^\circ, 62.8^\circ, 68.9^\circ, 70.4^\circ$ correspond to the pure anatase phase of TiO_2 . The XRD spectrum of the ZnO reference sample (Figure S1) exhibited a wurtzite (hexagonal phase) structure. The entire XRD peaks are in excellent conformity with the (JCPDS) card No. 36-1451.

The SEM micrographs in Figure 2 show the morphology of different LDH indicating the apparent effect of different metal cations in the LDH matrix. As seen in Figure 2a, the Zn-Ti LDH showed the highest prevalence of flake-like structures among all three samples, and the structure of these flakes was more defined in comparison to the other LDH. These flakes were stacked in an orderly manner, with an average length of 200–300 nm. They clearly exhibited the hierarchical structure of the LDH containing interlayer pores of varied sizes. The presence of these flakes to form a porous structure correlated well with the work described by Shao et al. [5].

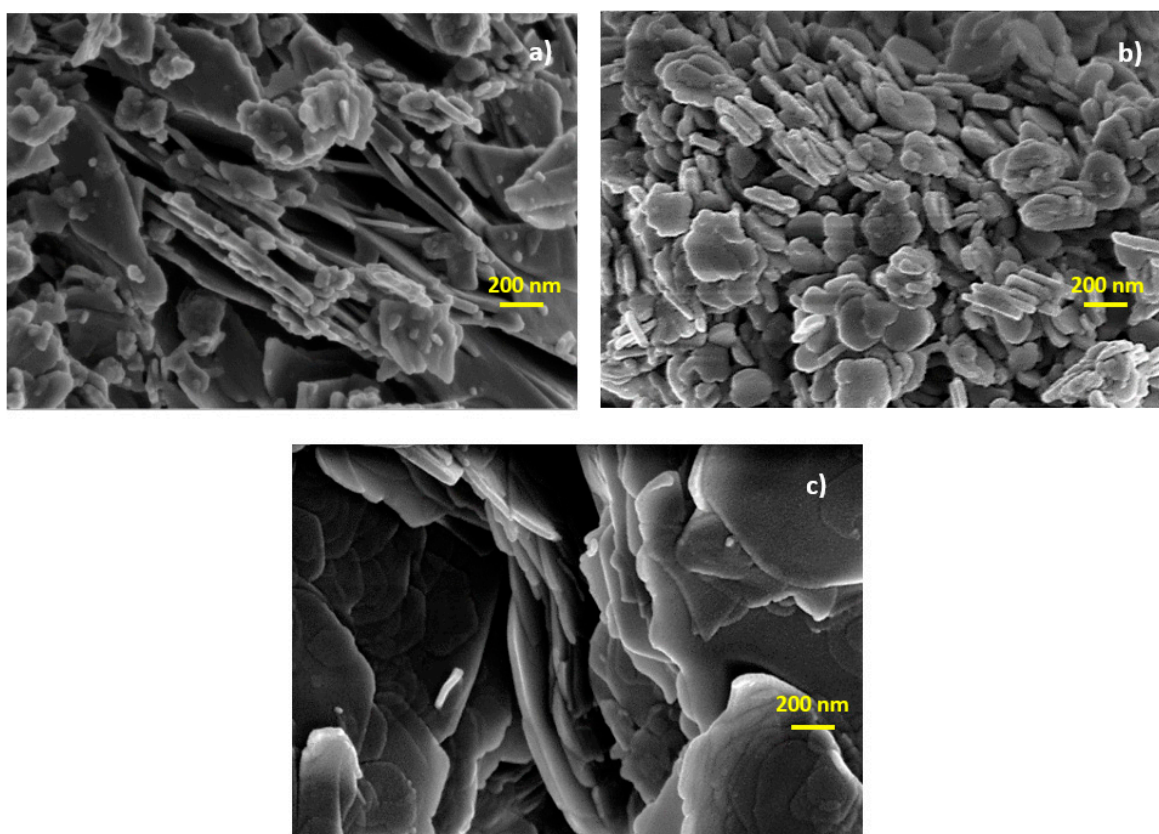


Figure 2. SEM images of (a) Zn-Ti LDH, (b) Zn-Al LDH and (c) Mg-Al LDH.

The morphology of the Zn-Al LDH (Figure 2b) was not as rigid and flakey as Zn-Ti LDH. These particles appeared to be more aggregated and smaller in comparison to the Zn-Ti LDH, with few particles bearing any resemblance to a nano-flake. This indicated that the substitution of Ti^{4+} with Al^{3+} in the LDH structure affected the overall morphology of the particles [5,31]. The incorporation of Al^{3+} caused more aggregation of particles, which may be due to the difference in electrostatic attraction within the LDH. SEM micrograph of Mg-Al LDH (Figure 2c) showed characteristic flake-like morphology, with flakes larger than those of Zn-Ti LDH and Zn-Al LDH but aggregated like Zn-Al LDH [31]. The average size of these flakes was between 900 nm and 2 μm . The difference in morphology and lack of “dessert rose” appearance could be due to the differences in synthesis conditions [10,31], as well as in the nature of the cations present. Naseem et al. [32] observed large and thin platelets for Mg-Al LDH, and this correlates with what was seen in this current study. It

was also reported that the platelet size was influenced by the amount and nature of the transition metal within the LDH.

The surface morphology of TiO_2 was analyzed by SEM analysis (Figure S2 in the Supplementary Materials) where the particles showed a spherical shape with some level of aggregation. The particle size was in the range of 90–110 nm. ZnO samples consisted of wurtzite ZnO nanoparticles with sizes of 100 to 500 nm and irregular morphologies (Figure S2).

FTIR provided information about the interlayer anions present in each of the LDH. Figure 3 shows the FTIR spectra for Zn-Ti LDH, Zn-Al LDH, and Mg-Al LDH. As seen in Figure 3a, the broad peak occurred at approximately 3295 cm^{-1} , a slight shift from the expected values in the literature; however, this still corresponded to the OH stretching mode due to intercalated water in the LDH layers [33,34]. In Figure 3b,c, the OH stretching mode was at 3407 cm^{-1} and 3448 cm^{-1} , respectively. The shift observed for the Zn-Ti LDH could be ascribed to the integration of a tetravalent ion into the structure [9]. The electronegativity value of Ti^{4+} is 1.59, in comparison to the electronegativity of Al^{3+} , which is 1.50. This difference in electronegativity affects the electron density on the O-H band (M-OH), thereby causing a shift to lower wavenumbers [14,35]. Furthermore, Zn-Ti (Figure 3a) LDH exhibited peak broadening of the OH stretching band, which may be due to the coordination of the OH groups to Ti^{4+} [14,34].

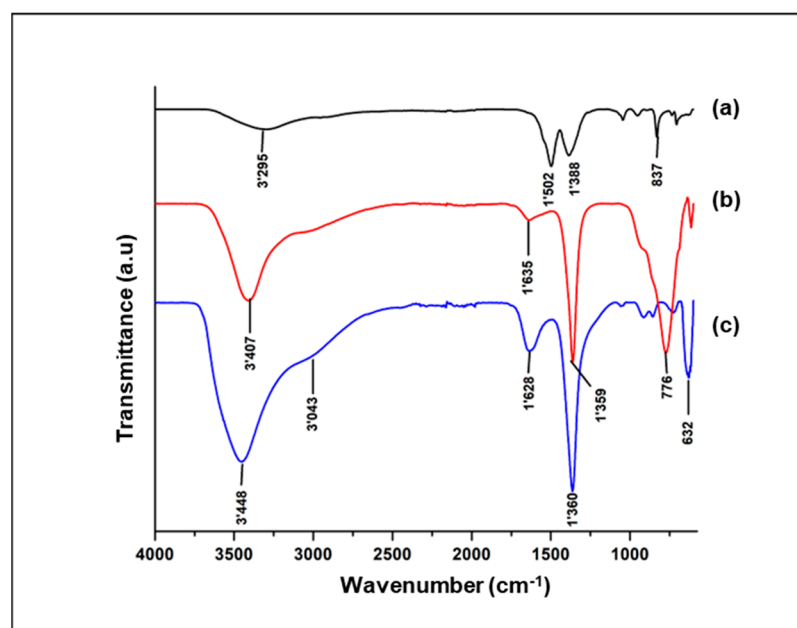


Figure 3. FTIR Spectra of (a) Zn-Ti LDH, (b) Zn-Al LDH and (c) Mg-Al LDH.

The O-H bending vibrational mode of water at approximately 1600 cm^{-1} was only observed for Zn-Al and Mg-Al, Figure 3b,c, respectively. This proves that the quantity of water present within the Zn-Ti LDH is far less in comparison to Mg-Al and Zn-Al. This could be attributed to the differences in drying conditions: Zn-Ti was dried in a vacuum oven at $120\text{ }^\circ\text{C}$, while Zn-Al was dried in a conventional air oven at $60\text{ }^\circ\text{C}$. The internal bonding between Zn^{2+} and Ti^{4+} could also contribute to a lower amount of interlayer water [28,33,34].

Figure 3 shows a strong band at approximately 1360 cm^{-1} for both LDH containing Al^{3+} , which is coherent with the conclusions of Gevers et al. [33] and Klopogge and Frost [36] on the existence of carbonate anion in the interlayer. This was further confirmed by a study by Sakr et al. [37]. In comparison, the band for Zn-Ti LDH (Figure 3a) is shifted to 1388 cm^{-1} , which might be attributed to the ν_3 of the interlayer monodentate carbonate species [36]. The presence of a double band for this sample was indicative of a lowering of

symmetry of the carbonate anions from D_{3d} to C_{2v} symmetry [4,14,27]. For Zn-Al LDH, a strong band with a shoulder at 776 cm^{-1} and 927 cm^{-1} corresponded to the ν_2 mode of the carbonate. The Mg-Al LDH had a sharp band at 632 cm^{-1} , due to the ν_4 mode of carbonate. Zn-Ti LDH had a weak band at 837 cm^{-1} , indicating the ν_2 mode of the carbonate anion [38]. This shift was attributed to the incorporation of Ti^{4+} [14]. Given that Zn-Ti LDH was synthesized in the absence of an inert atmosphere, these bands can be due to the carbonate anions rather than nitrate anions [39]. However, because the precursor salts contained nitrate salts, the presence of nitrate anion should not be ruled out.

The surface characteristics, such as specific surface area, pore volume, and pore diameter of the synthesized LDH, were performed by BET and BJH procedures (Table 1). LDH-type materials are generally described by their external surface mesoporosity because N_2 has a diameter that is greater than the interlayer space present in the LDH. Therefore, the value obtained for pore volume correlated with the interparticle pores. The porosity of the material could be affected by the presence of different cations, which alter the microscopic structure [14,40].

Table 1. Summary of BET surface area, pore volume, and pore diameter of LDH samples.

Sample	BET Surface Area (m^2/g)	Pore Volume (cm^3/g)	Pore Diameter (nm)
Zn-Ti LDH	77.02 ± 1.58	0.13 ± 0.003	6.75 ± 0.29
Zn-Al LDH	36.61 ± 1.66	0.12 ± 0.01	23.49 ± 4.43
Mg-Al LDH	15.73 ± 1.30	0.08 ± 0.002	20.62 ± 0.59

As observed in Table 1, Zn-Ti LDH showed the highest BET surface area together with the highest pore volume. By substituting a tetravalent ion into the matrix, the isotherm changed from type IV to type II (Figure S3) due to the changes in the surface morphology of the particles [14,40]. Hence, it may be concluded that the incorporation of a tetravalent cation rather than a trivalent cation facilitated an increase in the overall surface area given the differences in electrostatic attraction.

The thermal stability of the synthesized LDH was analysed using TGA as seen in Figure 4, and all samples exhibited multi-step degradation events. The thermal stability of LDH is strongly dependent on the nature of the cation, interlayer anion, and the experimental parameters used for the synthesis [41,42].

Dependent on the nature of the cations incorporated, oxidation or reduction (redox) processes may occur during heating. In the absence of redox processes, thermal decompositions are known to occur in four steps: (1) loss of surface adsorbed water, occurring below $80\text{ }^\circ\text{C}$; (2) removal of interlayer water; (3) dehydroxylation; and (4) removal of interlayer anion [41,42].

The highest weight loss temperature typically represents the third and fourth degradation step of dehydroxylation and loss of interlayer anion [35,36]. Reports in the literature have shown that for a Zn-Al LDH, the loss of carbonates occurs between approximately 230 and $460\text{ }^\circ\text{C}$ [4,34]. Figure 4 showed that this step occurred at approximately 230 – $457\text{ }^\circ\text{C}$ for Zn-Al LDH. In comparison, for Mg-Al LDH this was around 237 – $438\text{ }^\circ\text{C}$, and for Zn-Ti LDH between 270 and $486\text{ }^\circ\text{C}$. The temperature range indicative of dehydroxylation and the loss of carbonates varied among LDH materials due to the variations in the electrostatic interactions between host layers and the carbonate groups. The higher temperature observed for Zn-Ti LDH implied a stronger interaction between carbonate anions and the brucite layer, which is consistent with a smaller interlayer spacing that was observed by XRD analysis [28,34]. In the case of Zn-Al, additional decomposition events were observed beyond $450\text{ }^\circ\text{C}$ and may be due to the decomposition of mixed metal oxides [43]. The existence of ZnO in the PXRD results affirmed the latter. Further deviations in temperature ranges were subject to differences in the electronegativity of the cations, which affected

the electrostatic interactions between the brucite layers, thereby either retaining or losing cations more readily [34,44].

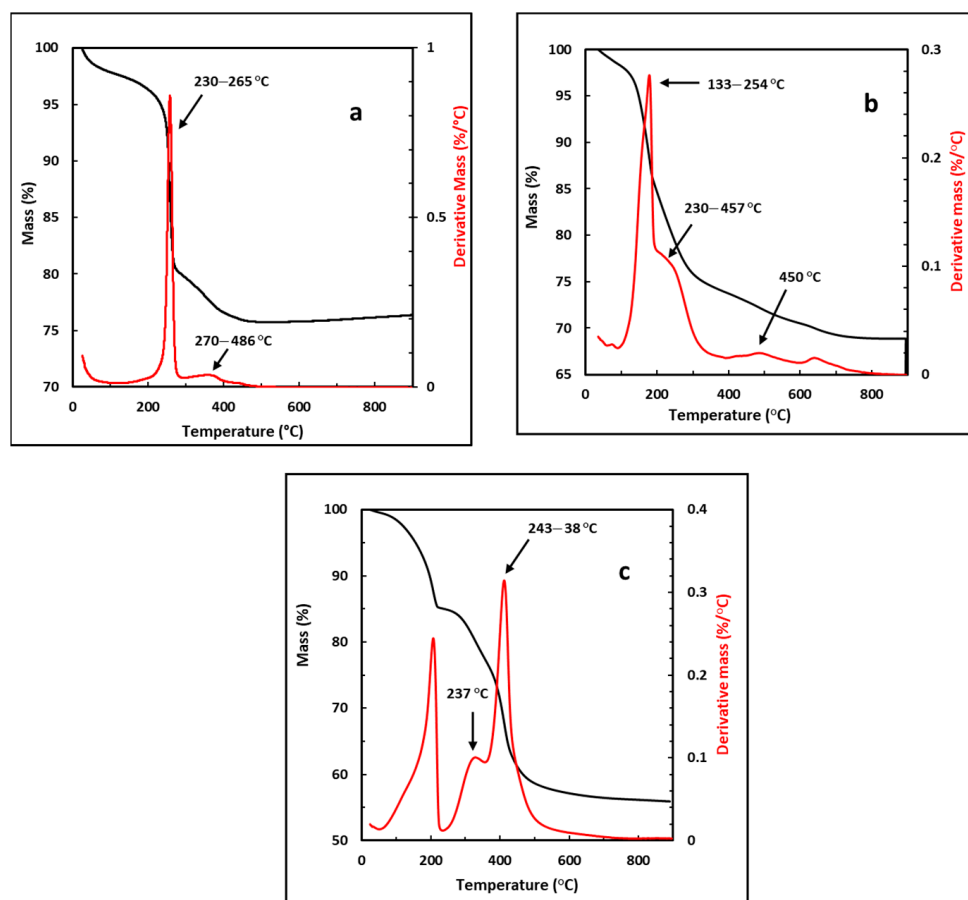


Figure 4. TGA and DTG curves for (a) Zn-Ti LDH, (b) Zn-Al LDH, and (c) Mg-Al LDH.

The properties of these thermal transitions or degradation steps, namely, temperature and mass loss, depend on the metal content in each LDH [41,42]. The results showed that the incorporation of different cations within the LDH structure indeed affected the overall properties—specifically, the thermal stability of the LDH. Zn-Ti LDH was the most thermally stable LDH as it experienced a mass loss at a relatively higher temperature. The increased thermal stability could be attributed to the differences in the drying conditions and synthetic parameters, as well as the difference in electrostatic interactions between the metal cation and the interlayer anion group [4,27,28,41,42].

3.2. Optical Properties of LDH

Figure 5 presents the DRUV-Vis spectra for Zn-Ti, Zn-Al, and Mg-Al LDH. The reflectance capability of each of the LDH differed significantly owing to the incorporation of different cations into the LDH structure. Zn-Al LDH exhibited the best reflectance capabilities in the visible region, with maximum reflectance recorded at approximately 98%, in comparison to Zn-Ti LDH and Mg-Al LDH, which had maximum reflectance of 91% and 45%, respectively.

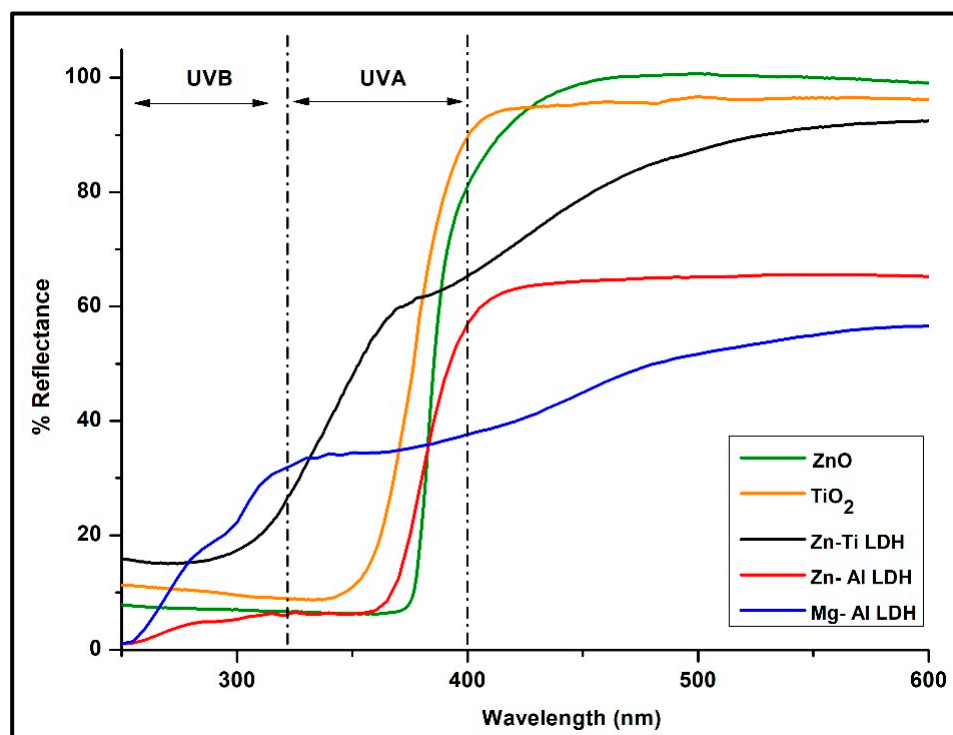


Figure 5. Diffuse Reflectance spectra for synthesized LDHs and references (ZnO and TiO₂).

As seen in Figure 5, it was apparent that, on average, Zn-Ti LDH exhibited higher levels of UVA reflectance in comparison to Mg-Al and Zn-Al LDH. The average reflectance values recorded within this range are 49%, 34.47%, and 18.36%, respectively, for Zn-Ti, Zn-Al, and Mg-Al LDH.

It is noteworthy that the UVA reflectance of Zn-based LDH was higher than that of Mg-Al LDH, which could be assigned to the presence of Zn²⁺ in the LDH structure [9,45]. The higher UVA reflectance exhibited by Zn-Ti LDH may be accounted for the synergistic effect of both Ti⁴⁺ and Zn²⁺ within the LDH structure [46–49]. It is also noticeable from Figure 5 that, in comparison to Zn-Al LDH (3.16%) and Mg-Al LDH (11.07%), Zn-Ti LDH (16.6%) showed greater capability for UVB reflectance as well. It may thus be concluded that the presence of Zn within the LDH structure improved the UV reflectance properties of the LDH. However, when we compare Zn-Ti and Zn-Al LDH, the incorporation of Ti⁴⁺ improved the overall UV reflection capacity further, particularly in the UVA range.

Kubelka–Munk (K–M) analysis was conducted (Figure S4), to convert reflectance values into equivalent absorption coefficients. Tauc plots were derived from K–M curves and were used for band gap determination (Figure S5, Table 2). The band gaps obtained for the references TiO₂ and ZnO were 3.23 eV and 3.27 eV, respectively, which agreed well with the reported values [9,50]. It is clear from Table 2 that the band gap of the Zn-Ti LDH is higher than those of the reference samples. However, the band gap of 3.74 eV did not correlate well with the previously reported value of 3.06 eV by Shao et al. [5].

Table 2. The band gap values obtained for LDH and reference samples.

Sample	Band Gap (eV)
Mg-Al LDH	4.75
Zn-Al LDH	4.5
Zn-Ti LDH	3.72
TiO ₂	3.23
ZnO	3.27

The band gap value of 4.5 and 4.75 eV obtained for Zn-Al and Mg-Al LDH correlated well with the literature [28,49]. The Mg-Al LDH had the largest band gap among all three LDHs. The difference in band gap values obtained between the LDH proved that the incorporation of different metal cations influenced the overall optical properties. The incorporation of Ti^{4+} within the LDH matrix led to a substantial reduction in the band gap in comparison to Al^{3+} . However, the coupling of Mg^{2+} with Al^{3+} resulted in a broader band gap which may be attributed to the band edge placement and work function of this LDH [49].

3.3. Photochemical Properties of LDH

The photocatalytic properties of the synthesized LDH were analyzed by observing the photodegradation of MB over a period of 4 h. The inherent adsorption of MB on different LDH was measured prior to photocatalytic testing [50–52]. Only minimal surface adsorption of MB on LDH was observed in the absence of UV, and the equilibrium concentration were 0.013, 0.004, and 0.029 g/L, respectively, for Zn-Ti, Zn-Al, and Mg-Al LDH.

Figure 6 shows the extent of MB photodegradation for LDH materials and references under UVR of wavelength 254 nm and 365 nm for 4 h. TiO_2 was the most photoreactive material under both wavelengths, while Mg-Al and Zn-Al LDH exhibited weaker photocatalytic properties. Both TiO_2 and ZnO presented elevated levels of photocatalytic activity with rapid rates of MB degradation over the 4 h UVR exposure period. After 4 h, the solution containing the references had changed from blue to a murky white solution, while the solution containing LDH remained colored. Given the lower band gaps of TiO_2 and ZnO, it was expected that these samples would exhibit higher photocatalytic activity under these wavelengths [53].

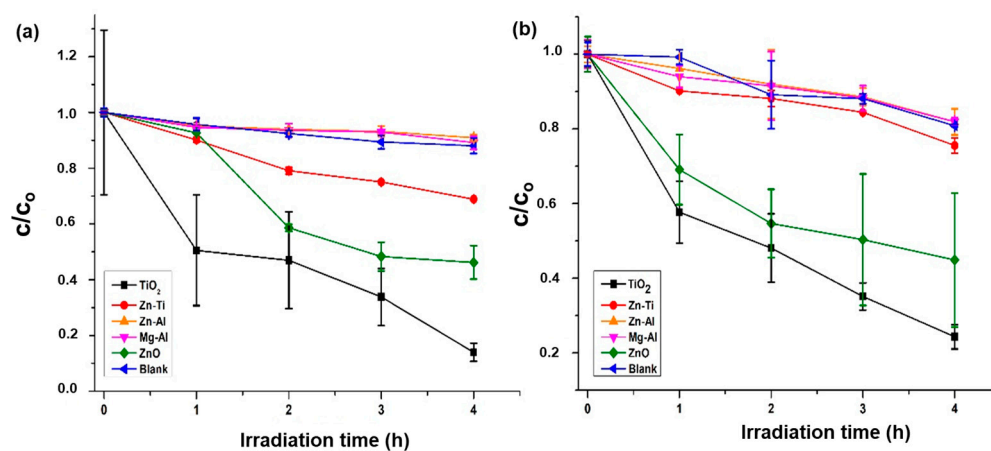


Figure 6. Photodegradation of MB references under (a) 254 nm and (b) 365 nm.

From Figure 6, it was evident that Mg-Al LDH exhibited the lowest photocatalytic activity at each wavelength, which may be attributed to its wide band gap of 4.75 eV. Owing to its lower band gap of 3.72 eV, it was expected that Zn-Ti LDH would exhibit higher photocatalytic activity than Zn-Al LDH (4.5 eV), and our results concurred with these assumptions. Despite the presence of ZnO in both LDH materials, the enhanced photocatalytic activity of Zn-Ti LDH could be credited to the presence of Ti within the structure [5,43,54]. However, in comparison to the metal oxide references, all three LDH showed significantly lower photoreactivity under both high-energy and low-energy UV radiations.

The presence of these recombination centers might justify the decreased photocatalytic activity of Zn-Ti and Zn-Al LDH [9]. The existence of Ti^{4+} and Al^{3+} could allow for the creation of localized energy levels, which acted as recombination centers. These recombination centers prevented the generation of holes in the valence band, and this ultimately inhibited the formation of ROS [55], and hence, the photocatalytic activity. A study by

Zhao et al. [56] further supports this observation as they indicated that the photocatalytic activity of an LDH material may be increased by raising the molar ratio of Zn atoms, while an increase in Al atoms decreased the photocatalytic activity. Figure 7 shows our proposed degradation pathway for LDH where the absence of a hole (h^+) prevents the formation of radical species.

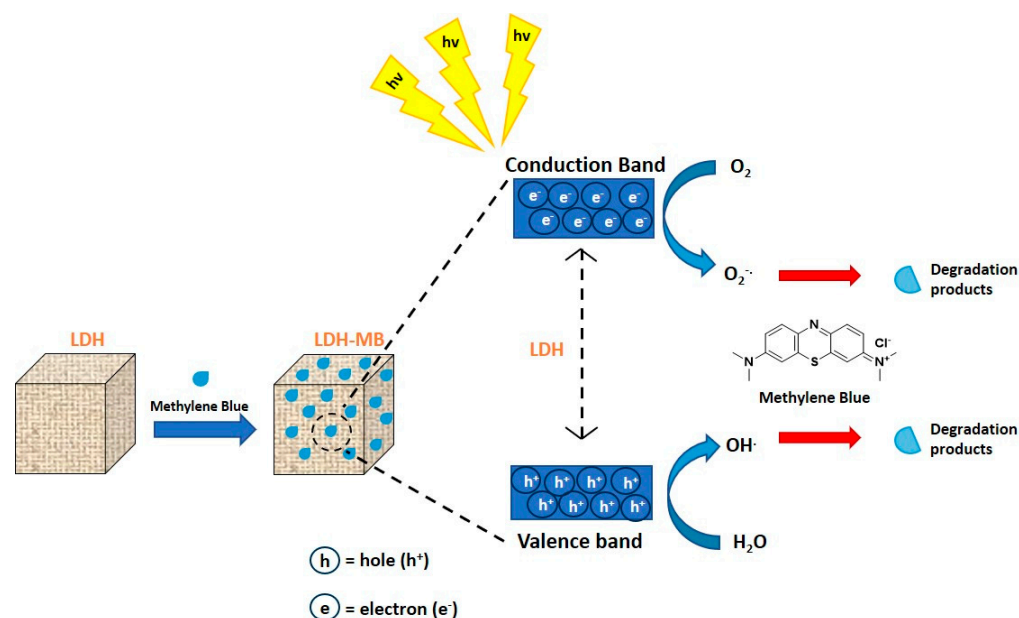


Figure 7. Proposed pathway of photocatalytic degradation of Methylene Blue by LDH.

3.4. In Vitro Sun Protection Factor (SPF) Testing

Following the favorable photocatalytic results obtained, SPF tests were conducted to determine whether they were suitable for potential use in sunscreen formulations. According to the diffuse reflectance data (Figure 5), Mg-Al LDH did not exhibit good UV reflectance capabilities like Zn-Al and Zn-Ti LDH, and hence was not suitable for use as a physical inorganic UV filter. Therefore, *in vitro* SPF testing was carried out only for formulations containing Zn-Ti and Zn-Al LDH.

The results in Table 3 show the average SPF and UVA-PF values measured for formulations containing 2 wt% Zn-Ti and Zn-Al LDH. The average SPF value obtained Zn-Ti LDH was 6.11, whereas the UVA-PF was 2.65 with a UVA balance of 41%. The corresponding values obtained for Zn-Al LDH were 4.29, 3.82, and 70%, respectively. The average critical wavelength measured was 384 nm and 387 nm for Zn-Ti and Zn-Al LDH. Given that the mean critical wavelength exceeded 370 nm, the claim of “Broad Spectrum” was valid. Furthermore, given that the UVA Balance was greater than 33% and the mean critical wavelength exceeded 370 nm, the claim of “UVA Protection” was also valid for both LDH [57–59].

Nur et al. [60] prepared 4-aminobenzoic acid intercalated Zn-Al LDH for sunscreen application. Although no SPF evaluation was conducted in this study, they concluded that the material prevented harmful and carcinogenic effects on the skin [60]. Several articles have highlighted the benefit of incorporating various organic UV filters into the Zn-Ti LDH interlayer to obtain slow-release characteristics. Also, in these instances, the SPF values of the formulations were never reported [61,62].

Madikizela et al. [63] suggested an SPF of 1.18 for natural clay mineral-containing formulations employing Mansur’s method. The group found that the natural clay could be used for beautification and detoxification while providing low UV coverage. The study concluded that the low UV coverage warranted further addition of additives such as TiO_2 [63]. A study by Abbas et al. [64] investigated the UV capabilities of calcium silicate, a

naturally occurring material in the soil of South Asian regions. This work reported an SPF of 37.94, using Mansur's method, for the 5 wt% calcium silicate in a formulation [64].

Table 3. *In vitro* SPF for synthesized Zn-Ti LDH (2 wt%) and Zn-Al LDH (2 wt%).

	Zn-Ti LDH (2 wt%)			Zn-Al LDH (2 wt%)		
	SPF (Mean)	UVA-PF (Pre-Irradiation)	UVA-PF	SPF (Mean)	UVA-PF (Pre-Irradiation)	UVA-PF
Plate 1	6.31	2.84	2.59	4.35	3.85	3.74
Plate 2	6.23	2.84	2.60	4.37	3.86	3.76
Plate 3	5.96	2.85	2.72	4.24	3.87	3.87
Plate 4	6.11	2.84	2.67	4.18	3.89	3.90
Average	6.15 ± 0.132	2.84 ± 0.004	2.65 ± 0.053	4.29 ± 0.078	3.87 ± 0.015	3.82 ± 0.069

As per a recent critical review, LDH materials are cost-effective and ever-evolving materials that offer a great alternative to current commercially available sunscreen formulations. The review highlighted the need for further research into the varying metal combinations to improve greater loading while inhibiting the leaching of active materials [17]. Our study clearly demonstrates lower photoreactivity along with good UV reflection capacity of Zn-based LDH in comparison to the commercial metal oxide counterparts. The formulations containing Zn-Ti and Zn-Al LDH were aesthetically pleasing and showed higher SPF values in comparison to other reported natural clay mineral sunscreens.

4. Concluding Remarks

The study demonstrated a strong impact of the nature of precursor cations on the structural, optical, and photochemical characteristics of LDH. The significantly lower photochemical activity was observed for the LDH in comparison to the currently used inorganic UV filters such as TiO₂ and ZnO, which is favorable for their use in safer photoprotective formulations. The incorporation of tetravalent titanium within an LDH structure altered the band gap, which ultimately translated to a favorable SPF. From this study, it was observed that Zn-Ti and Zn-Al LDH may be considered for further use in sunscreen formulations due to their demonstrated UV-shielding properties. As no organic additives were incorporated into the LDH in this study, there was no risk of additive leaching, which was previously encountered in other studies and resulted in delayed exposure of these photocatalytic materials to photodegradation conditions. There is an inordinate demand for innovative inorganic UV filters from the personal care sector that better talk to UVR shielding, photo-stability, "broad" or "full" spectrum protection, and safety, with fewer side effects and no skin penetrability. Furthermore, this study revealed the prospects of LDH for such applications.

Supplementary Materials: The following supporting information can be downloaded at: <https://www.mdpi.com/article/10.3390/cosmetics10040100/s1>, Table S1: Relative amounts of contents for oil/water formulations; Figure S1: XRD spectra of TiO₂ and ZnO; Figure S2: SEM images of (a) TiO₂ and (b) ZnO; Figure S3: N₂—adsorption isotherms for LDHs synthesized with different metal cations; Figure S4: Kubelka-Munk plot of different LDH and references (ZnO and TiO₂); Figure S5: Tauc plots indicating the band Gap of (a) Zn-Ti LDH, (b) Zn-Al LDH and (c) Mg-Al LDH.

Author Contributions: Formal analysis, investigation, writing—original draft preparation, O.P.E.; Conceptualization, methodology, validation, supervision, funding acquisition, S.K.P.; Writing—review, and editing, S.K.P., S.S.R. and M.G. All authors have read and agreed to the published version of the manuscript.

Funding: This research was funded by the Department of Science and Innovation, South Africa [C6EEM29], and O.P.E was supported by the National Research Foundation, South Africa [Grant No. 100849].

Institutional Review Board Statement: Not applicable.

Informed Consent Statement: Not applicable.

Data Availability Statement: Data obtained in this study are available in this manuscript.

Acknowledgments: The authors wish to thank CSIR and the Department of Science and Innovation South Africa for the research support. The authors also extend their gratitude to AMKA Products (Pty) Ltd. (South Africa) for providing ingredients for the preparation of formulations. The CeNAM characterization facility is also acknowledged for supporting the research project.

Conflicts of Interest: The authors declare no conflict of interest.

References

1. Cavallaro, G.; Caruso, M.R.; Milioto, S.; Fakhrollin, R.; Lazzara, G. Keratin/alginate hybrid hydrogels filled with halloysite clay nanotubes for protective treatment of human hair. *Int. J. Bio. Macromol.* **2022**, *222*, 228–238. [[CrossRef](#)] [[PubMed](#)]
2. Cavallaro, G.; Milioto, S.; Konnova, S.; Fakhrollina, G.; Akhatova, F.; Lazzara, G.; Fakhrollin, R.; Lvov, Y. Halloysite/keratin nanocomposite for human hair photoprotection coating. *ACS Appl. Mater. Interfaces* **2020**, *12*, 24348–24362. [[CrossRef](#)] [[PubMed](#)]
3. Daniel, S.; Thomas, S. Layered double hydroxides: Fundamentals to applications. In *Layered Double Hydroxide Polymer Nanocomposites*; Woodhead Publishing: Sawston, UK, 2020; pp. 1–76. [[CrossRef](#)]
4. Duan, X.; Evans, D.G. Layered Double Hydroxides. In *Structure and Bonding*; Duan, X., Evans, D.G., Eds.; Springer: Beijing, China, 2005; pp. 3–70. [[CrossRef](#)]
5. Shao, M.; Han, J.; Wei, M.; Evans, D.G.; Duan, X. The Synthesis of Hierarchical Zn-Ti Layered Double Hydroxide for Efficient Visible-Light Photocatalysis. *Chem. Eng. J.* **2011**, *168*, 519–524. [[CrossRef](#)]
6. Evans, D.G.; Slade, R.C.T. *Structural Aspects of Layered Double Hydroxides BT—Layered Double Hydroxides*; Duan, X., Evans, D.G., Eds.; Springer: Berlin/Heidelberg, Germany, 2006; pp. 1–87. [[CrossRef](#)]
7. De Roy, A.; Forano, C.; Besse, J.P. Layered Double Hydroxides: Synthesis and Post-Synthesis Modification. In *Layered Double Hydroxides: Present and Future*; Nova Science Publishers Inc.: New York, NY, USA, 2001; pp. 1–37. [[CrossRef](#)]
8. Mishra, G.; Dash, B.; Pandey, S. Layered Double Hydroxides: A Brief Review from Fundamentals to Application as Evolving Biomaterials. *Appl. Clay Sci.* **2018**, *153*, 172–186. [[CrossRef](#)]
9. Egambaram, O.P.; Pillai, S.K.; Lategan, M.; Ray, S.S. Nanostructured Zn-Ti Layered Double Hydroxides with Reduced Photocatalytic Activity for Sunscreen Application. *J. Nanoparticle Res.* **2019**, *21*, 53. [[CrossRef](#)]
10. Bukhtiyarova, M.V. A Review on Effect of Synthesis Conditions on the Formation of Layered Double Hydroxides. *J. Solid State Chem.* **2019**, *269*, 494–506. [[CrossRef](#)]
11. Starukh, G. Photocatalytically Enhanced Cationic Dye Removal with Zn-Al Layered Double Hydroxides. *Nanoscale Res. Lett.* **2017**, *12*, 391. [[CrossRef](#)]
12. Gevers, B.R.; Naseem, S.; Sheppard, C.J.; Leuteritz, A.; Labuschagné, F.J.W.J. Modification of Layered Double Hydroxides Using First-Row Transition Metals for Superior UV-Vis-NIR Absorption and the Influence of the Synthesis Method Used. In *ChemRxiv*; Cambridge Open Engage: Cambridge, UK, 2020. [[CrossRef](#)]
13. Sahu, R.K.; Mohanta, B.S.; Das, N.N. Synthesis, Characterization and Photocatalytic Activity of Mixed Oxides Derived from ZnAlTi Ternary Layered Double Hydroxides. *J. Phys. Chem. Solids* **2013**, *74*, 1263–1270. [[CrossRef](#)]
14. Seftel, E.M.; Popovici, E.; Mertens, M.; Van Tendeloo, G.; Cool, P.; Vansant, E.F. The Influence of the Cationic Ratio on the Incorporation of Ti⁴⁺ in the Brucite-like Sheets of Layered Double Hydroxides. *Microporous Mesoporous Mater* **2008**, *111*, 12–17. [[CrossRef](#)]
15. Fivenson, D.; Sabzevari, N.; Qiblawi, S.; Blitz, J.; Norton, B.B.; Norton, S.A. Sunscreens: UV filters to protect us: Part 2-Increasing awareness of UV filters and their potential toxicities to us and our environment. *Int. J. Women's Dermatol.* **2021**, *7*, 45–69. [[CrossRef](#)]
16. Wright, C.Y.; du Preez, D.J.; Millar, D.A.; Norval, M. The epidemiology of skin cancer and public health strategies for its prevention in southern Africa. *Int. J. Environ. Res. Public Health* **2020**, *17*, 1017. [[CrossRef](#)]
17. Franco, J.G.; Ataide, J.A.; Ferreira, A.H.P.; Mazzola, P.G. Lamellar Compounds Intercalated with Anions with Solar Protection Function: A Review. *J. Drug Deliv. Sci. Technol.* **2020**, *59*, 101869. [[CrossRef](#)]
18. Ng, W.K.; Martincigh, B.S. Applied Clay Science Review Article A Critical Review on Layered Double Hydroxides: Their Synthesis and Application in Sunscreen Formulations. *Appl. Clay Sci.* **2021**, *208*, 106095. [[CrossRef](#)]
19. Pillai, S.K.; Kleyi, P.; De Beer, M.; Mudaly, P. Layered Double Hydroxides: An Advanced Encapsulation and Delivery System for Cosmetic Ingredients—an Overview. *Appl. Clay Sci.* **2020**, *199*, 105868. [[CrossRef](#)]
20. Cunha, V.R.R.; de Souza, R.B.; da Fonseca Martins, A.M.C.R.P.; Koh, I.H.J.; Constantino, V.R.L. Accessing the biocompatibility of layered double hydroxide by intramuscular implantation: Histological and microcirculation evaluation. *Sci. Rep.* **2016**, *6*, 30547. [[CrossRef](#)]
21. Rojas, R.; Mosconi, G.; Zanin, J.P.; Gil, G.A. Layered double hydroxide applications in biomedical implants. *Appl. Clay Sci.* **2022**, *224*, 106514. [[CrossRef](#)]

22. Kim, H.J.; Lagarrigue, P.; Oh, J.M.; Soulié, J.; Salles, F.; Cazalbou, S.; Drouet, C. Biocompatible MgFeCO₃ Layered Double Hydroxide (LDH) for Bone Regeneration—Low-Temperature Processing through Cold Sintering and Freeze-Casting. *Bioengineering* **2023**, *10*, 734. [[CrossRef](#)]
23. Li, P.; Huang, Y.; Fu, C.; Jiang, S.X.; Peng, W.; Jia, Y.; Peng, H.; Zhang, P.; Manzie, N.; Mitter, N.; et al. Eco-friendly biomolecule-nanomaterial hybrids as next-generation agrochemicals for topical delivery. *EcoMat* **2021**, *3*, e12132. [[CrossRef](#)]
24. Meng, Y.; Zhang, B.; Su, J.; Han, J. Bioinspired Design of LDH-Based Mobile Building Materials with Enhanced Mechanical and Ultraviolet-Shielding Performance. *Macromol. Mater. Eng.* **2019**, *304*, 1900276. [[CrossRef](#)]
25. Shi, Y.; Gui, Z.; Yu, B.; Yuen, R.K.K.; Wang, B.; Hu, Y. Graphite-like Carbon Nitride and Functionalized Layered Double Hydroxide Filled Polypropylene-Grafted Maleic Anhydride Nanocomposites: Comparison in Flame Retardancy, and Thermal, Mechanical and UV-Shielding Properties. *Compos. Part B Eng.* **2015**, *79*, 277–284. [[CrossRef](#)]
26. Cao, T.; Xu, K.; Chen, G.; Guo, C. Poly (Ethylene Terephthalate) Nanocomposites with a Strong UV-Shielding Function Using UV-Absorber Intercalated Layered Double Hydroxides. *Rsc. Adv.* **2013**, *3*, 6282–6285. [[CrossRef](#)]
27. Rives, V. Layered Double Hydroxides: Present and Future. *Appl. Clay Sci.* **2001**, *22*, 75–76.
28. Ahmed, A.A.A.; Talib, Z.A.; Bin Hussein, M.Z.; Zakaria, A. Zn-Al Layered Double Hydroxide Prepared at Different Molar Ratios: Preparation, Characterization, Optical and Dielectric Properties. *J. Solid State Chem.* **2012**, *191*, 271–278. [[CrossRef](#)]
29. Costantino, U.; Marmottini, F.; Nocchetti, M.; Vivani, R. New Synthetic Routes to Hydrotalcite-Like Compounds—Characterisation and Properties of the Obtained Materials. *Eur. J. Inorg. Chem.* **1998**, *10*, 1439–1446. [[CrossRef](#)]
30. Seftel, E.M.; Popovici, E.; Mertens, M.; De Witte, K.; Van Tendeloo, G.; Cool, P.; Vansant, E.F. Zn-Al Layered Double Hydroxides: Synthesis, Characterization and Photocatalytic Application. *Microporous Mesoporous Mater.* **2008**, *113*, 296–304. [[CrossRef](#)]
31. Wang, M.; Bao, W.J.; Wang, J.; Wang, K.; Xu, J.J.; Chen, H.Y.; Xia, X.H. A Green Approach to the Synthesis of Novel “Desert Rose Stone”-like Nanobiocatalytic System with Excellent Enzyme Activity and Stability. *Sci. Rep.* **2014**, *4*, 1–8. [[CrossRef](#)]
32. Naseem, S.; Gevers, B.; Boldt, R.; Labuschagné, F.J.W.J.; Leuteritz, A. Comparison of Transition Metal (Fe, Co, Ni, Cu, and Zn) Containing Tri-Metal Layered Double Hydroxides (LDHs) Prepared by Urea Hydrolysis. *RSC Adv.* **2019**, *9*, 3030–3040. [[CrossRef](#)]
33. Gevers, B.R.; Naseem, S.; Leuteritz, A.; Labuschagné, F.J.W.J. Comparison of Nano-Structured Transition Metal Modified Tri-Metal MgMAI-LDHs (M = Fe, Zn, Cu, Ni, Co) Prepared Using Co-Precipitation. *RSC Adv.* **2019**, *9*, 28262–28275. [[CrossRef](#)]
34. Saber, O.; Tagaya, H. New Layered Double Hydroxide, Zn-Ti LDH: Preparation and Intercalation Reactions. *J. Incl. Phenom. Macrocycl. Chem.* **2003**, *45*, 109–116. [[CrossRef](#)]
35. Xu, Z.P.; Braterman, P.S. Synthesis, Structure and Morphology of Organic Layered Double Hydroxide (LDH) Hybrids: Comparison between Aliphatic Anions and Their Oxygenated Analogs. *Appl. Clay Sci.* **2010**, *48*, 235–242. [[CrossRef](#)]
36. Klopogge, J.T.; Frost, R.L. Fourier Transform Infrared and Raman Spectroscopic Study of the Local Structure of Mg-, Ni-, and Co-Hydrotalcites. *J. Solid State Chem.* **1999**, *146*, 505–515. [[CrossRef](#)]
37. Sakr, A.A.E.; Zaki, T.; Elgabry, O.; Ebiad, M.A.; El-Sabagh, S.M.; Emara, M.M. Mg-Zn-Al LDH: Influence of Intercalated Anions on CO₂ Removal from Natural Gas. *Appl. Clay Sci.* **2018**, *160*, 263–269. [[CrossRef](#)]
38. Benício, L.P.F.; Silva, R.A.; Lopes, J.A.; Eulálio, D.; dos Santos, R.M.M.; De Aquino, L.A.; Vergütz, L.; Novais, R.F.; Da Costa, L.M.; Pinto, F.G.; et al. Layered Double Hydroxides: Nanomaterials for Applications in Agriculture. *Rev. Bras. Cienc. Do Solo* **2015**, *39*, 1–13. [[CrossRef](#)]
39. Olanrewaju, J.; Newalkar, B.L.; Mancino, C.; Komarneni, S. Simplified Synthesis of Nitrate from of Layered Double Hydroxide. *Mater. Lett.* **2000**, *45*, 307. [[CrossRef](#)]
40. Seftel, E.M.; Niarchos, M.; Vordos, N.; Nolan, J.W.; Mertens, M.; Mitropoulos, A.C.; Vansant, E.F.; Cool, P. LDH and TiO₂/LDH-Type Nanocomposite Systems: A Systematic Study on Structural Characteristics. *Microporous Mesoporous Mater.* **2015**, *203*, 208–215. [[CrossRef](#)]
41. Rives, V. Study of Layered Double Hydroxides by Thermal Methods. In *Layered Double Hydroxides: Present and Future*; Nova Science Publishers Inc.: New York, NY, USA, 2001; pp. 127–151.
42. Rives, V. Characterisation of Layered Double Hydroxides and Their Decomposition Products. *Mater. Chem. Phys.* **2002**, *75*, 19–25. [[CrossRef](#)]
43. Theiss, F.L.; Ayoko, G.A.; Frost, R.L. Thermogravimetric Analysis of Selected Layered Double Hydroxides. *J. Therm. Anal. Calorim.* **2013**, *112*, 649–657. [[CrossRef](#)]
44. Saber, O.; Tagaya, H. Preparation of a New Nano-Layered Materials and Organic-Inorganic Nano-Hybrid Materials, Zn-Si LDH. *J. Porous Mater.* **2009**, *16*, 81–89. [[CrossRef](#)]
45. Manaia, E.B.; Kaminski, R.C.K.; Corrêa, M.A.; Chiavacci, L.A. Inorganic UV Filters. *Braz. J. Pharm. Sci.* **2013**, *49*, 201–209. [[CrossRef](#)]
46. Egambaram, O.P.; Kesavan Pillai, S.; Sinha Ray, S. Materials Science Challenges in Skin UV Protection: A Review. *Photochem. Photobiol.* **2019**, *96*, 779–797. [[CrossRef](#)]
47. Shi, L.; Shan, J.; Ju, Y.; Aikens, P.; Prud'homme, R.K. Nanoparticles as Delivery Vehicles for Sunscreen Agents. *Colloids Surf. A Physicochem. Eng. Asp.* **2012**, *396*, 122–129. [[CrossRef](#)]
48. Serpone, N.; Dondi, D.; Albini, A. Inorganic and Organic UV Filters: Their Role and Efficacy in Sunscreens and Suncare Products. *Inorg. Chim. Acta* **2007**, *360*, 794–802. [[CrossRef](#)]

49. Xu, S.-M.; Pan, T.; Dou, Y.-B.; Yan, H.; Zhang, S.-T.; Ning, F.-Y.; Shi, W.-Y.; Wei, M. Theoretical and Experimental Study on M^{II} M^{III}-Layered Double Hydroxides as Efficient Photocatalysts toward Oxygen Evolution from Water. *J. Phys. Chem. C* **2015**, *119*, 18823–18834. [[CrossRef](#)]
50. Starukh, G.; Rozovik, O.; Oranska, O. Organo/Zn-Al LDH Nanocomposites for Cationic Dye Removal from Aqueous Media. *Nanoscale Res. Lett.* **2016**, *11*, 228. [[CrossRef](#)]
51. Mahjoubi, F.Z.; Khalidi, A.; Abdennouri, M.; Barka, N. Zn–Al Layered Double Hydroxides Intercalated with Carbonate, Nitrate, Chloride and Sulphate Ions: Synthesis, Characterisation and Dye Removal Properties. *J. Taibah Univ. Sci.* **2017**, *11*, 90–100. [[CrossRef](#)]
52. Starukh, G.N. Zn-Al Layered Double Hydroxides for Adsorption and Photocatalytic Removal of Cationic Dye. *Chem. Phys. Technol. Surf.* **2016**, *7*, 379–388. [[CrossRef](#)]
53. Smijs, T.G.; Pavel, S. Titanium Dioxide and Zinc Oxide Nanoparticles in Sunscreens: Focus on Their Safety and Effectiveness. *Nanotechnol. Sci. Appl.* **2011**, *4*, 95–112. [[CrossRef](#)]
54. Tayade, R.J.; Natarajan, T.S.; Bajaj, H.C. Photocatalytic Degradation of Methylene Blue Dye Using Ultraviolet Light Emitting Diodes. *Ind. Eng. Chem. Res.* **2009**, *48*, 10262–10267. [[CrossRef](#)]
55. Ali, A.; Muhammad, A. Doped Metal Oxide (ZnO) and Photocatalysis: A Review. *J. Pak. Inst. Chem. Eng. J.* **2012**, *40*, 11–19. [[CrossRef](#)]
56. Zhao, G.; Zou, J.; Li, C.; Yu, J.; Jiang, X.; Zheng, Y.; Hu, W.; Jiao, F. Enhanced Photocatalytic Degradation of Rhodamine B, Methylene Blue and 4-Nitrophenol under Visible Light Irradiation Using TiO₂/MgZnAl Layered Double Hydroxide. *J. Mater. Sci. Mater. Electron.* **2018**, *29*, 7002–7014. [[CrossRef](#)]
57. Sayer, R.M.; Staniland, P.; Stansfield, G.L. Importance of Broad Spectrum Inorganic Sunscreens in Preventing UV and Near-UV Induced Free Radical Damage to the Skin. *Cosmet. Sci. Technol.* **2013**, 95–102.
58. Pelizzo, M.; Zattra, E.; Nicolosi, P.; Peserico, A.; Garoli, D.; Alaibac, M. In Vitro Evaluation of Sunscreens: An Update for the Clinicians. *ISRN Dermatol.* **2012**, *2012*, 352135. [[CrossRef](#)]
59. Santos Caetano, J.P.; Abarca, A.P.; Guerato, M.; Guerra, L.; Schalka, S.; Perez Simão, D.C.; Vila, R. SPF and UVA-PF Sunscreen Evaluation: Are There Good Correlations among Results Obtained in Vivo, in Vitro and in a Theoretical Sunscreen Simulator? A Real-Life Exercise. *Int. J. Cosmet. Sci.* **2016**, *38*, 576–580. [[CrossRef](#)]
60. Nur, I.; Abdul, F.; Siti, A.; Sarijo, H.; Sakina, F.; Rajidi, M.; Yahaya, R.; Musa, M. Synthesis and Characterization of Novel 4-Aminobenzoate Interleaved with Zinc Layered Hydroxide for Potential Sunscreen Application. *J. Porous Mater.* **2019**, *26*, 717–722. [[CrossRef](#)]
61. Li, Y.; Tang, L.; Zhou, W.; Wang, X. Fabrication of Intercalated p-Aminobenzoic Acid into Zn-Ti Layered Double Hydroxide and Its Application as UV Absorbent. *Chin. Chem. Lett.* **2016**, *27*, 1495–1499. [[CrossRef](#)]
62. Li, Y.; Tang, L.; Ma, X.; Wang, X.; Zhou, W.; Bai, D. Synthesis and Characterization of Zn-Ti Layered Double Hydroxide Intercalated with Cinnamic Acid for Cosmetic Application. *J. Phys. Chem. Solids* **2017**, *107*, 62–67. [[CrossRef](#)]
63. Madikizela, L.M.; Nkwentsha, N.; Mlunguza, N.Y. Physicochemical Characterization and In Vitro Evaluation of the Sun Protection Factor of Cosmetic Products Made from Natural Clay Material. *S. Afr. J. Chem.* **2017**, *70*, 113–119. [[CrossRef](#)]
64. Abbas, N.; Manzoor, S.; Saeed, S.; Muhammad, S.; Tariq, M.; Akhtar, Z.; Saira, N.; Yasmin, G. Investigation of Calcium Silicate as a Natural Clay-Based Sunblock: Formulation and Characterization. *Photodermat. Photoimmun. Photomed.* **2021**, *37*, 39–48. [[CrossRef](#)]

Disclaimer/Publisher’s Note: The statements, opinions and data contained in all publications are solely those of the individual author(s) and contributor(s) and not of MDPI and/or the editor(s). MDPI and/or the editor(s) disclaim responsibility for any injury to people or property resulting from any ideas, methods, instructions or products referred to in the content.